IET Image Processing

Research Article

FuSENet: Fused Squeeze-and-Excitation Network for Spectral-Spatial Hyperspectral Image Classification

ISSN 1751-8644
doi: 0000000000
www.ietdl.org

Swalpa Kumar Roy[1] *Shiv Ram Dubey*[2] *Subhrasankar Chatterjee*[3] *and Bidyut Baran Chaudhuri*[4]

[1] Department of Computer Science & Engineering, Jalpaiguri Government of Engineering College, West Bengal-735102, India
[2] Computer Vision Group, Indian Institute of Information Technology, Sri City, Chittoor, Andhra Pradesh-517646, India
[3] Department of Computer Science & Engineering, Indian Institute of Technology, Kharagpur, West Bengal-721302, India
[4] Computer Vision and Pattern Recognition Unit, Indian Statistical Institute, Kolkata-700108, India
** E-mail: swalpa@cse.jgec.ac.in, srdubey@iiits.in, sc1933@cse.jgec.ac.in, bbc@isical.ac.in*

Abstract: Deep learning based approaches have become very prominent in recent years due to its outstanding performance as compared to the hand-extracted feature based methods. Convolutional Neural Network (CNN) is a type of deep learning architecture to deal with the image/video data. Residual Network (ResNet) and Squeeze and Excitation Network (SENet) are among recent developments in CNN for image classification. However, the performance of SENet is depends on the squeeze operation done by global pooling, which sometimes may lead to poor performance. In this paper, we propose a bilinear fusion mechanism over different types of squeeze operation such as global pooling and max pooling. The excitation operation is performed using the fused output of squeeze operation. We used to model the proposed fused squeeze and excitation network with the residual unit and name it as `FuSENet`. Here the classification experiments are performed over benchmark hyperspectral Image (HSI) datasets. The experimental results confirm the superiority of the proposed `FuSENet` method with respect to the state-of-the-art methods. The source code of the complete system is made publicly available at `https://github.com/swalpa/FuSENet`.

1 Introduction

Deep learning based techniques have become the recent trend of research due to their great performance in practice. Convolutional Neural Network (CNN) has emerged as very popular architecture to solve the image recognition problem [1]. The first revolutionary work in this area was AlexNet CNN model [1] which won the ImageNet large-scale object recognition challenge [2] in 2012. Since then various variants of CNN have been proposed for different problems such as ResNet [3], SENet [4] for image classification; R-CNN [5], Fast-RCNN [6], Faster-RCNN [7] for object detection; Mask-RCNN [8] for image segmentation; Local Bit-plane Decoded Alexnet Descriptor [9] for biomedical image retrieval; Dual CNN [10] for depth estimation; HybridSN [11], Genetaic Neural Network [12] for hyperspectral image classification; RCCNet [13] for colon cancer classification, etc. The recent works over CNN are image classification [14], medical image analysis, [15], deep hashing [16], hyperspectral image (HSI) classification [17], [18], face anti-spoofing [19], [20], texture classification [21], etc.

The residual based CNN, called ResNet [3], is a widely used network due to the skip connection. The skip connection of ResNet facilitates the better optimization of network using gradient descent method as it provides the super highway for gradient flow during back-propagation. Several variants of ResNet have been investigated such as ResNeXt [22], DenseNet [23], etc. Moreover, ResNet is also used for the experimentation over loss functions [24] and optimisation methods [25]. The Squeeze and Excitation Network (SENet) [4] is one of the very recent breakthrough in deep learning community. The SENet tries to enhance the inter-channel relationship between different channels of CNN activation's. Basically, first it squeezes the volume using global pooling across spatial dimension, then an excitation factor is generated using a small neural network over squeezed data, and finally the channels of input activation volume are excited with this excitation factor. This type of network might be better suited for hyperspectral image classification problem as it contains many channels at different wavelengths. Thus, in order to reduce the effect of redundancy, the automatic prioritisation of intermediate channels are needed which is provided by the excitation scores of such network. But a major problem with SENet is associated with only one type of pooling for squeezing which may miss the relevant information. We tackle this problem by fusing the excitation scores, computed using different squeeze networks.

The hyperspectral image (HSI) contains the information in several spectral bands of imaging [26]. The HSI has wide range of real-world applications such as earth observations and land cover classification such as greenery detection, environment analysis, crop analysis, and many more [27], [28]. The CNNs have also shown very promising performance for HSI classification task [29], [30], [31]. Some researchers have also explored the fusion in CNN such as Dual-path network [32], Convolutional feature fusion network [33], Deep feature fusion network [34], 3D-2D CNN fusion [11], spatial-spectral squeeze-and-excitation residual network (SSSERN) [35], and spectral-spatial squeeze-and-excitation residual bag-of-features learning (S3EResBoF) [36] for HSI classification. These methods incorporate the feature fusion at the feature level. However, we aim to incorporate the fusion within a layered residual block.

In this paper, we propose a fusion of squeeze and excitation network (`FuSENet`) for HSI classification. The original SENet [4] contains only one squeeze and excitation block. However, the proposed `FuSENet` uses fusion of two bilinear squeeze and excitation network with different squeezing strategies. The proposed method captures the channel relationship in multiple ways to make the excitation factor more relevant. The main contribution is as follows:

1. A `FuSENet` model is proposed by fusing the excitation scores from multiple squeezing channels.
2. Two squeezing channels are considered to generate the excitation scores through Global pooling and Max pooling, respectively.
3. The fusion of multiple squeeze and excitation scores are better suited for HSI data as it has multiple channels.
4. The proposed fused scores priorities the important channels towards better training and convergence.
5. An extensive HSI classification experiments are performed to show the improved performance using proposed `FuSENet` model.

© The Institution of Engineering and Technology 2019

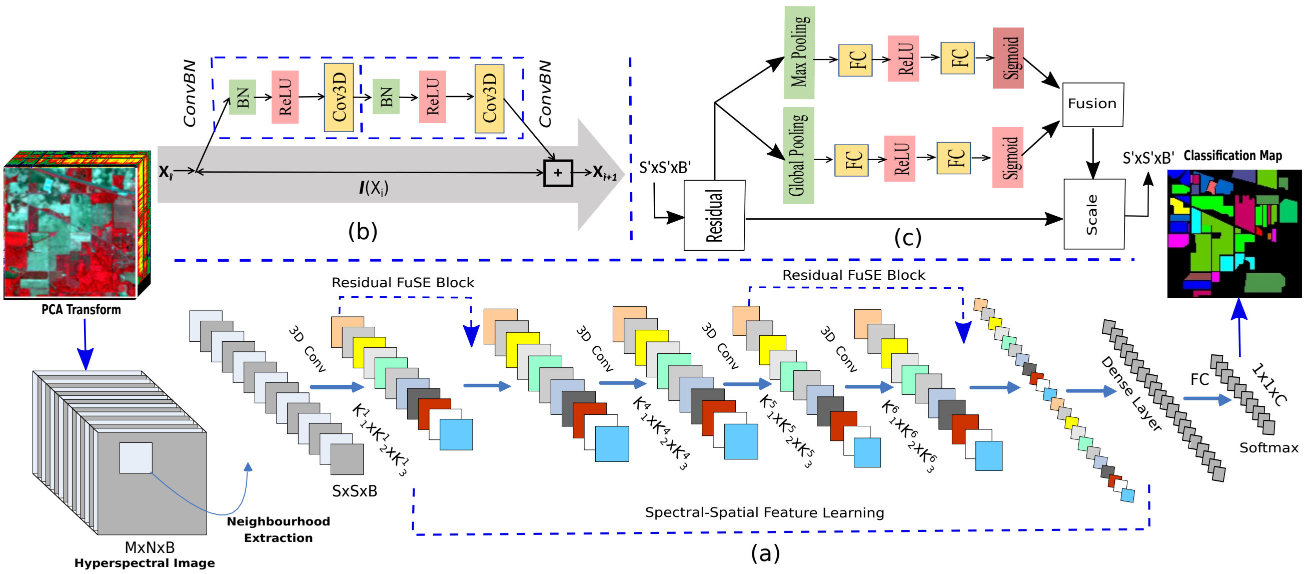

Fig. 1: The proposed `FuSENet` end-to-end learning model for HSI classification. The 3D blocks of dimension $S \times S \times B$ are extracted and used for training and testing purpose. The kernel settings are as follows: $K_1^{1/4/5/6} = 15$, $K_2^{1/4/5/6} = 15$, and $K_3^{1/4/5/6} = 5$, respectively and all the layer use 32 numbers of kernels.

6. The weight of proposed `FuSENet` model is reduced because less no. of blocks are needed as compared to the SENet.

This paper is organized as follows: Section 2 presents the proposed `FuSENet` model; Section 3 carries the experiments and results analysis; and Section 4 concludes the paper.

2 Proposed `FuSENet` Model

We propose a `FuSENet` model in this paper for hyperspectral image (HSI) classification. Motivated from the nature of HSI data (i.e., many no. of channels in input data), we make use the squeeze and excitation network (SENet) [4] in the proposed method. Basically, the poposed `FuSENet` model fuses the excitation scores computed through different squeeze channels. The proposed `FuSENet` model is described in Fig. 1. Let us consider a 3D hyperspectral image, $\mathbf{X}_{org} \in \mathcal{R}^{M \times N \times D}$, where M, N, and D are the width, height, and spectral dimension, respectively. In order to remove the spectral redundancy, first we employ the principal component analysis (PCA) and reduce the number of spectral bands from D to B. The output of PCA is denoted by $\mathbf{X}_r \in \mathcal{R}^{M \times N \times B}$, where B is the reduced spectral bands after PCA. Further, $\mathbf{X}_r$ is divided into several regions, defined as $\mathbf{x}_{i,j,k} \in \mathcal{R}^{S \times S \times B}$ centered at pixel (i, j) with S as the spatial dimension. The center of each region $\mathbf{x}_{i,j} = [x_{i,j,1}, \ldots x_{i,j,B}]$ is labeled as $Y = (y_1, y_2, \ldots y_C)$, where C is the number of classes. These regions along with the ground truth class labels of its center are used for training and validation in classification framework.

We propose a fusion of squeeze and excitation network (`FuSENet`) by considering the ResNet [3] as the base model. The batch normalization (BN) [37] is used followed by a 3D convolutional layer within the residual blocks. The conventional residual blocks shown in Fig. 1(b) and can be formulated as:

$$\begin{aligned} X_{out}^{l+2} &= \mathcal{I}(X_{in}^{l}) + \mathcal{F}(X_{in}^{l}; \theta, \Omega) \\ \mathcal{F}(X_{in}^{l}; \theta, \Omega) &= \phi(X_{in}^{l+1}) * W^{l+2} + b^{l+2} \\ X_{in}^{l+1} &= \phi(X_{in}^{l}) * W^{l+1} + b^{l+1} \end{aligned} \tag{1}$$

where $X_{in}^{l} \in \mathcal{R}^{S \times S \times B}$ and $X_{out}^{l+2} \in \mathcal{R}^{S' \times S' \times B'}$ represent the input and output feature maps. The residual function is defined by $\mathcal{F}(.)$, parameterized by θ and Ω to represent the convolutional parameter of two subsequent layers and $*$ and ϕ represent the convolution operation and activation function, respectively. Every residual block is followed by the proposed fused squeeze-and-excitation (FuSE) block (as depicted by Residual FuSE Block in Fig. 1(c)). The output of FuSE block is used to re-calibrate the input channels of that block. Basically, the FuSE block uses Global Average Pooling (GAP) and Global Max Pooling (GMP) for squeezing operation as given by

$$\begin{aligned} SQ_{avg}^{c} &= \frac{1}{S' \times S'} \sum_{i=1}^{S'} \sum_{j=1}^{S'} (f_{i,j,c}) \\ SQ_{max}^{c} &= max_{i,j=1}^{S',S'} (f_{i,j,c}) \end{aligned} \tag{2}$$

where $f \in \mathcal{R}^{S' \times S' \times B'}$ is the input feature map to FuSE block, $f_{i,j,c}$ is the feature at (i, j) position in c^{th} channel and SQ_{avg}^{c} and SQ_{max}^{c} are the squeezed values for c^{th} channel using global Average and Max pooling, respectively. Basically, the squeeze operation extracts the channel-wise information. Moreover, the global pooling will retail the information in global context, whereas the max pooling will retain the information in local context. The excitation networks are used to prioritize the features extracted by the squeeze operation. The uses of multiple squeeze channels ensures that the final excitation scores should not be biased towards global or local information.

The excitation factors (EX_{avg} and EX_{max}) corresponding to SQ_{avg} and SQ_{max}, respectively, are computed as

$$EX_{avg} = \sigma(W_{2,avg}, \delta(W_{1,avg}, SQ_{avg})) \tag{3}$$

and

$$EX_{max} = \sigma(W_{2,max}, \delta(W_{1,max}, SQ_{max})) \tag{4}$$

where σ and δ refer to the Sigmoid and ReLU activation functions, respectively [4], $\mathbf{W}_1 \in \mathcal{R}^{\frac{B}{r} \times B}$ and $\mathbf{W}_2 \in \mathcal{R}^{B \times \frac{B}{r}}$ are the weights of 1^{st} and 2^{nd} dense layers of FuSE block, and r is a constant factor by which at first the dimension of squeezed data is decreased and then inceased before Sigmoid layer. In the proposed FuSE block, we

Table 1 The class-wise varying training, validation and test samples and the performance measured in term of OA, Kappa, and AA metric over Indian Pines.

Indian Pines (IP)					
Class	Name	Training	Validation	Test	Accuracy
1	Alfalfa	6	2	38	100
2	Corn-no till	214	71	1143	98.47
3	Corn-min till	124	41	665	98.53
4	Corn	35	11	191	98.56
5	Grass-pasture	72	24	387	99.95
6	Grass-trees	109	36	585	99.60
7	Grass-pasture-mowed	4	1	23	98.75
8	Hay-windrowed	71	23	384	99.40
9	Oats	3	1	16	100
10	Soybean-no till	145	48	779	98.54
11	Soybean-min till	368	122	1965	98.42
12	Soybean-clean	88	29	476	98.94
13	Wheat	30	10	165	98.66
14	Woods	189	63	1013	98.98
15	Buildings-Grass-Trees-Drives	57	19	310	100
16	Stone-Steel-Towers	13	4	76	98.36
	OA				99.01 ± 0.1
	Kappa				98.60 ± 0.1
	AA				98.64 ± 0.1
	Total	1528	505	8216	

Table 2 The class-wise varying training, validation and test samples and the performance measured in term of OA, Kappa, and AA metric over University of Pavia.

University of Pavia (UP)					
Class	Name	Training	Validation	Test	Accuracy
1	Asphalt	994	331	5306	99.89
2	Meadows	2797	932	14920	99.93
3	Gravel	314	104	1681	98.75
4	Trees	459	153	2452	98.71
5	Painted metal sheets	201	67	1077	98.69
6	Bare Soil	754	251	4024	99.76
7	Bitumen	199	66	1065	99.94
8	Self-Blocking Bricks	552	184	2946	98.31
9	Shadows	142	47	758	100
	OA				99.42 ± 0.2
	Kappa				99.21 ± 0.3
	AA				99.33 ± 0.2
	Total	6412	2135	34229	

Table 3 The class-wise varying training, validation and test samples and the performance measured in term of OA, Kappa, and AA metric over Salinas Scene.

Salinas Scene (SA)					
Class	Name	Training	Validation	Test	Accuracy
1	Brocoli_green_weeds_1	301	100	1608	100
2	Brocoli_green_weeds_2	558	186	2982	100
3	Fallow	296	98	1582	99.63
4	Fallow_rough_plow	209	69	1116	99.21
5	Fallow_smooth	401	133	2144	100
6	Stubble	593	197	3169	100
7	Celery	536	178	2865	99.61
8	Grapes_untrained	1690	563	9018	99.97
9	Soil_vinyard_develop	930	310	4963	99.97
10	Corn_senesced_green_weeds	491	163	2624	99.95
11	Lettuce_romaine_4wk	160	53	855	100
12	Lettuce_romaine_5wk	289	96	1542	99.84
13	Lettuce_romaine_6wk	137	45	734	98.88
14	Lettuce_romaine_7wk	160	53	857	99.96
15	Vinyard_untrained	1090	363	5815	99.59
16	Vinyard_vertical_trellis	271	90	1446	98.59
	OA				99.68 ± 0.2
	Kappa				99.74 ± 0.1
	AA				99.69 ± 0.1
	Total	8112	2697	43320	

fuse the excitation factors to compute the final scaling factor (s) as

$$s_c = F(EX^c_{avg}, EX^c_{max}) \tag{5}$$

where EX^c_{avg} and EX^c_{max} are the excitation factors for c^{th} channel corresponding to the GAP and GMP, respectively, s_c is the scaling factor after fusion, and $F \in \{Sum, Prod, Max\}$ is the fusion strategy. The Sum, $Prod$, and Max are the summation, product, and maximum fusion strategies. As shown in Fig. 1(c), the final scaling factor is used to scale the FuSE block input can be re-formulated the residual block as:

$$X^{l+2}_{out}(i,j,c) = \mathcal{I}(X^l_{in}(i,j,c)) + s_c \times \mathcal{F}_c(X^l_{in}; \theta, \Omega) \tag{6}$$

where $\mathcal{F}_c$ represents the c^{th} channel of residual output, $X^{l+2}_{out}(i,j,c)$ is the final output from `FuSENet` block. Since, it is the channel-wise product of the scalar s_c and the feature map $\mathcal{F}_c(X^l_{in}; \theta, \Omega)$. Hence, the `FuSENet` block captures the importance of different channels and improves the inter-channel relationship. The *feature recalibration* using proposed FuSE block prioritizes the important channels using higher scaling factor and improves the feature representation produced by the residual network (ResNet) [38]. A dense layer and a softmax layer are used on the flattened output of the final Residual `FuSENet` Block as shown in Fig. 1.

3 Experiments and Discussion

A series of experiments are conducted to test the superiority of the proposed `FuSENet` model. The results are compared with state-of-the-art models such as SVMs [39], 2D-CNN [40], 3D-CNN [41], M3D-CNN [42], Two-CNN [43], SENet [4], Dual-path network (DPNet) [32], Convolutional feature fusion network (ConvFeaFuNet) [33], and Deep feature fusion network (DFeaFuNet) [34], respectively. The model is trained using RMSProp optimizer with a learning rate of 0.001 for 1000 epochs over each HSI data set. The categorical cross-entropy loss is minimized using backpropagation. Batch normalization (BN) and 50% of dropout are used to deal with over-fitting.

3.1 Hyperspectral Datasets

The Indian Pines (IP), University of Pavia (UP) and Salinas Scene (SA) HSI datasets* are used for experiments and analysis. The used **Indian Pines (IP) data set** [44] contains the images with 200 spectral bands and having spatial dimension of size 145 × 145 from 16 mutually exclusive vegetation classes. The used **University of Pavia (UP) dataset** consists of 610 × 340 pixel spatially with 103 spectral bands from 9 urban land-cover classes. The used **Salinas Scene (SA) dataset** comprises of the images of 512 × 217 spatial dimension and 200 spectral bands from 16 vegetation classes.

Once the proposed `FuSENet` is successfully trained under the above settings and can be checked the performance of the model over the test samples. To validate we have adopted three relevant measurement for calculating the classification performance. Overall Accuracy (OA) is determined by the sum of class-wise correctly classified pixels divided by the total number of presence test pixels; The class accuracy (CA) denotes the percentage of accurately classified samples in each category.

$$OA = \frac{\sum_{i=1}^{n} p_{ii}}{N} \times 100\% \tag{7}$$

$$CA = \frac{p_{ii}}{\sum_{i=1}^{n} p_{ij}} \times 100\% \tag{8}$$

where the total number of classes and the total number of pixels in the dataset are represented by n,and N respectively. p_{ii} represents the pixel which are perfectly classified and p_{ij} the pixels actually belonging to i^{th} class of the HSI data and during classification it was assigned into j^{th} class. Average Accuracy (AA) denotes sum of the class-wise accuracy divided by the number of classes presence in the dataset and can be calculated as,

$$AA = \frac{\sum_{i=1}^{n} CA_i}{n} \times 100\% \tag{9}$$

and Kappa Coefficient (kappa) is a another metric of statistical measurement which calculate mutual information between the ground

* *http://dase.grss-ieee.org/*

Table 4 The classification accuracies (%) in term of OA, Kappa, and AA using the proposed FuSENet methods with varying training data 10% and 20%, respectively.

Training Samples	Methods	Indian Pines Dataset			University of Pavia Dataset			Salinas Scene Dataset		
		OA	Kappa	AA	OA	Kappa	AA	OA	Kappa	AA
10%	SVM	81.67 ± 0.65	78.76 ± 0.77	79.84 ± 3.37	90.58 ± 0.47	87.21 ± 0.70	92.99 ± 0.36	94.46 ± 0.12	93.13 ± 0.34	93.01 ± 0.60
	2D-CNN	80.27 ± 1.2	78.26 ± 2.1	68.32 ± 4.1	96.63 ± 0.2	95.53 ± 1.0	94.84 ± 1.4	96.34 ± 0.3	95.93 ± 0.9	94.36 ± 0.5
	3D-CNN	82.62 ± 0.1	79.25 ± 0.3	76.51 ± 0.1	96.34 ± 0.2	94.90 ± 1.2	97.03 ± 0.6	85.00 ± 0.1	83.20 ± 0.7	89.63 ± 0.2
	M3D-CNN	81.39 ± 2.6	81.20 ± 2.0	75.22 ± 0.7	95.95 ± 0.6	93.40 ± 0.4	97.52 ± 1.0	94.20 ± 0.8	93.61 ± 0.3	96.66 ± 0.5
	Two-CNN	96.71 ± 0.1	96.10 ± 0.10	96.16 ± 0.12	97.71 ± 0.1	97.62 ± 0.1	97.45 ± 0.2	97.12 ± 0.30	96.98 ± 0.20	97.00 ± 0.20
	DPNet	96.04 ± 0.2	96.97 ± 0.07	96.93 ± 0.07	97.67 ± 0.1	97.58 ± 0.1	97.27 ± 0.2	97.97± 0.1	97.95 ± 0.1	98.11 ± 0.1
	ConvFeaFuNet	97.39 ± 0.4	97.16 ± 0.5	97.01 ± 0.5	97.72 ± 0.1	97.64 ± 0.2	97.20 ± 0.2	97.89 ± 0.1	97.83 ± 0.1	97.91 ± 0.1
	DFeaFuNet	97.45 ± 0.2	97.79 ± 0.2	97.61 ± 0.2	97.38 ± 0.3	96.93 ± 0.4	97.32 ± 0.3	98.74 ± 0.2	98.91 ± 0.1	98.88 ± 0.1
	SENet(GMP)	97.48 ± 0.3	97.84 ± 0.2	97.91 ± 0.3	97.56 ± 0.5	97.41 ± 0.4	97.47 ± 0.4	98.88 ± 0.1	98.93 ± 0.2	99.01 ± 0.1
	SENet(GAP)	97.62 ± 0.3	97.91 ± 0.2	97.88 ± 0.3	97.53 ± 0.6	97.48 ± 0.5	97.52 ± 0.5	99.11 ± 0.2	98.89 ± 0.2	99.06 ± 0.2
	FuSENet	**98.11 ± 0.2**	**98.25 ± 0.2**	**98.32 ± 0.2**	**98.65 ± 0.3**	**98.69 ± 0.3**	**98.68 ± 0.4**	**99.23 ± 0.1**	**98.97 ± 0.2**	**99.16 ± 0.1**
20%	SVM	86.24 ± 0.38	84.27 ± 0.45	83.15 ± 1.10	95.20 ± 0.13	93.63 ± 0.17	93.60 ± 0.14	94.15 ± 0.10	93.48 ± 0.11	97.23 ± 0.11
	2D-CNN	86.90 ± 1.3	85.01 ± 1.6	82.70 ± 1.0	96.02 ± 0.4	96.04 ± 0.3	95.10 ± 0.1	96.15 ± 0.6	95.71 ± 0.7	98.27 ± 0.2
	3D-CNN	89.23 ± 0.2	87.70 ± 0.3	87.87 ± 0.1	97.30 ± 0.3	96.22 ± 0.1	97.02 ± 0.1	94.54 ± 0.5	93.81 ± 0.3	96.79 ± 0.6
	M3D-CNN	93.67 ± 0.1	92.70 ± 0.3	93.60 ± 0.6	97.41 ± 0.2	96.05 ± 0.6	98.22 ± 0.1	94.92 ± 0.3	94.40 ± 0.1	97.28 ± 0.2
	Two-CNN	98.73 ± 0.2	98.71 ± 0.2	98.73 ± 0.2	98.72 ± 0.25	98.40 ± 0.17	98.45 ± 0.20	98.13 ± 0.43	98.01 ± 0.20	98.10 ± 0.20
	DPNet	98.84 ± 0.1	98.33 ± 0.1	98.42 ± 0.1	98.37 ± 0.1	98.32 ± 0.1	98.39 ± 0.2	98.27± 0.2	98.15 ± 0.1	98.21 ± 0.1
	ConvFeaFuNet	98.79 ± 0.3	98.46 ± 0.4	98.71 ± 0.3	98.51 ± 0.2	98.54 ± 0.2	98.57 ± 0.2	98.44 ± 0.1	98.48 ± 0.0	98.45 ± 0.0
	DFeaFuNet	98.75 ± 0.2	98.72 ± 0.2	98.49 ± 0.2	98.93 ± 0.3	98.91 ± 0.4	98.94 ± 0.3	98.98 ± 0.2	99.01 ± 0.1	98.96 ± 0.1
	SENet(GMP)	98.53 ± 0.6	98.27 ± 0.8	97.91 ± 1.5	99.05 ± 0.2	98.81 ± 0.2	98.86 ± 0.2	99.07 ± 0.3	99.19 ± 0.2	99.13 ± 0.2
	SENet(GAP)	98.76 ± 0.5	98.43 ± 0.7	98.20 ± 1.0	99.36 ± 0.1	99.20 ± 0.1	99.30 ± 0.1	99.50 ± 0.1	99.55 ± 0.1	99.40 ± 0.1
	FuSENet	**99.01 ± 0.1**	**98.60 ± 0.1**	**98.64 ± 0.1**	**99.42 ± 0.2**	**99.21 ± 0.3**	**99.33 ± 0.2**	**99.68 ± 0.2**	**99.74 ± 0.1**	**99.69 ± 0.1**

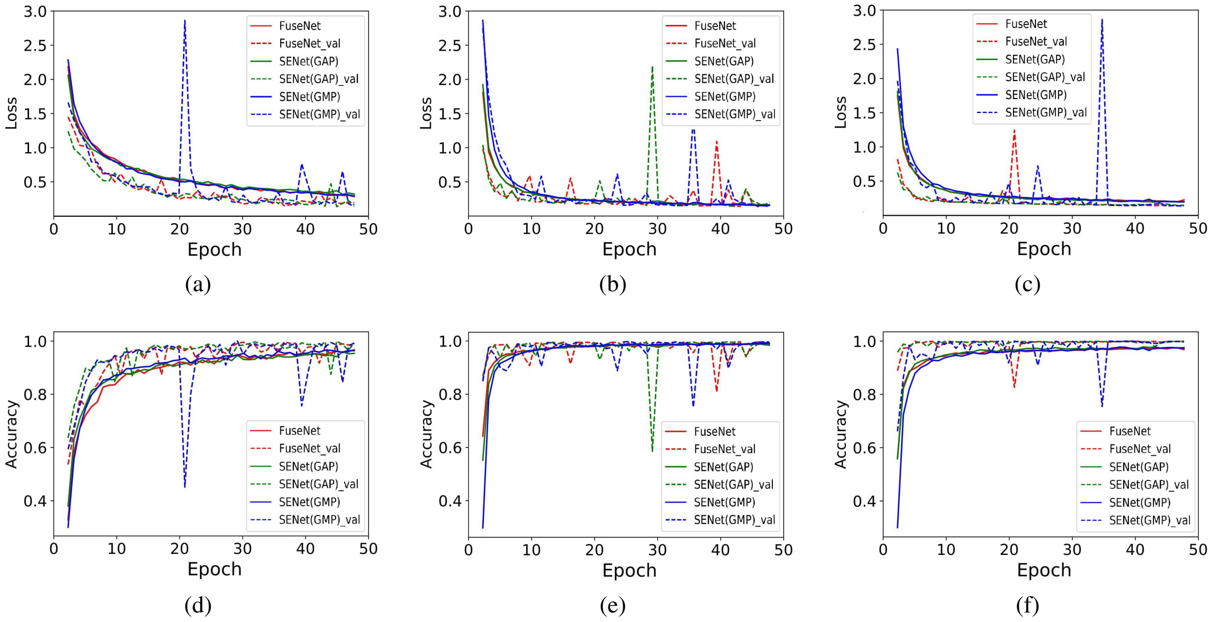

(a)

(b)

(c)

(d)

(e)

(f)

Fig. 2: (a)-(c) The convergence of loss vs epochs and (d)-(f) The accuracy vs epochs using the SENet(GAP), SENet(GMP) and `FuSENet` models over IP, UP and SA datasets, respectively.

truth map and predicted classification map and also shows a strong agreement. Which can be defined as follows,

$$kappa = \frac{N \sum_{i=1}^{n} p_{ii} - \sum_{i=1}^{n} p_i \sum_{j=1}^{n} p_j}{N^2 - \sum_{i=1}^{n} p_i \sum_{j=1}^{n} p_j} \tag{10}$$

where the diagonal elements of the corresponding confusion matrix, the total sum of the i^{th} row and total sum of the j^{th} column are represented by p_{ii}, p_i and p_j respectively.

In order to well explore in both the spectral and spatial context and to perform the unbiased comparison, various small spectral-spatial 3D input patches are extracted for each HSI datasets, such as 30 spectral bands are extracted with spatial window of sizes 15×15, and 13×13, for IP data set and similarly 15 spectral bands are extracted with spatial window of sizes 15×15, and 13×13, for both UP and SA data sets, respectively. In order to evaluate the effectiveness of the proposed `FuSENet`, the whole extracted 3D input patches are randomly selected into three sets viz., training, validation and testing. During the training 20%, and 10% available labeled 3D patches are selected from each class. In addition, unlabeled 5% available samples patches from each class was supplied for the model validation and the remaining samples for model testing. Moreover, to avoid the biases among different classes with imbalance samples, the experiments were repeated 10 times and the evaluated performance are reported in terms of mean±std value. The detail description of training, validation and testing along with class-wise classification accuracies i.e, OAs, AAs, and kappa coefficients are given in the Table 1, 2, and 3, respectively. In addition Table 4 shows the comparison with the well-known HSI classification methods under varying training samples i.e., 10% and 20% respectively. It is observed from the table that the proposed `FuSENet` model reaches consistent classification performance in both the scenario as compared to SVM, 2D-CNN, 3D-CNN, M3D-CNN, Two-CNN, DPNet, ConvFeaFuNet, DFeaFuNet, SENet(GMP), and SENet(GMP), respectively. The OAs achieved by SENet(GAP) model is higher than other compared spectral or spatial based methods since the method uses 3D convolution within the residual learning block and is capable to extract

Table 5 The performance of `FuSENet` using different fusion strategies such as addition (Sum), multiplication (Mul) and maximum (Max) over each dataset.

Training Samples	Methods	Indian Pines Dataset			University of Pavia Dataset			Salinas Scene Dataset		
		OA	Kappa	AA	OA	Kappa	AA	OA	Kappa	AA
20%	Sum	94.74 ± 0.2	94.56 ± 0.2	95.65 ± 0.2	96.39 ± 0.2	97.94 ± 0.2	96.49 ± 0.3	98.07 ± 0.1	98.39 ± 0.1	98.11 ± 0.1
	Multiply	95.31 ± 0.2	96.77 ± 0.3	95.41 ± 0.3	97.33 ± 0.2	97.45 ± 0.1	96.87 ± 0.2	98.12 ± 0.1	98.73 ± 0.2	98.25 ± 0.1
	Max	**99.01 ± 0.1**	**98.60 ± 0.1**	**98.64 ± 0.1**	**99.42± 0.2**	**99.21 ± 0.3**	**99.33 ± 0.2**	**99.68 ± 0.2**	**99.74 ± 0.1**	**99.69 ± 0.1**

Table 6 The influence of varying training samples (i.e., 20%, 10%, 5%) with respect to the spatial window of size ($S \times S$) (i.e., 15×15 and 13×13) over the performance of proposed `FuSENet` on Indian Pines (IP), Uinversity of Pavia (UP), and Salinas Scene (SA) datasets.

Training(%)	Window Size	Indian Pines Dataset			University of Pavia Dataset			Salinas Scene Dataset		
		OA	AA	Kappa	OA	AA	Kappa	OA	AA	Kappa
20%	15 x 15	**99.01 ± 0.1**	**98.60 ± 0.1**	**98.64 ± 0.1**	99.42± 0.2	99.21 ± 0.3	99.33 ± 0.2	**99.68 ± 0.2**	**99.74 ± 0.1**	**99.69 ± 0.1**
10%		98.11 ± 0.2	98.25 ± 0.2	98.32 ± 0.2	97.65 ± 0.3	97.69 ± 0.3	97.68 ± 0.4	99.23 ± 0.1	98.97 ± 0.2	99.16 ± 0.1
5%		93.48 ± 2.2	93.11 ± 2.1	91.27 ± 2.3	**99.58 ± 0.1**	**99.36 ± 0.1**	**99.44 ± 0.1**	99.14 ± 0.2	99.56 ± 0.1	99.04 ± 0.2
20%	13 x 13	**97.76 ± 0.4**	**97.45 ± 0.4**	**96.28 ± 0.4**	**99.77± 0.2**	**99.67± 0.2**	**99.69 ± 0.2**	**99.97 ± 0.0**	**99.97 ± 0.0**	**99.96 ± 0.0**
10%		96.14 ± 1.3	96.17 ± 1.2	95.45 ± 1.6	99.67 ± 0.2	99.62 ± 0.2	99.56 ± 0.2	99.94 ± 0.0	99.92 ± 0.0	99.93 ± 0.0
5%		93.48 ± 2.2	93.11 ± 2.1	91.27 ± 2.3	99.58 ± 0.1	99.36 ± 0.1	99.44 ± 0.1	99.14 ± 0.2	99.56 ± 0.1	99.04 ± 0.2

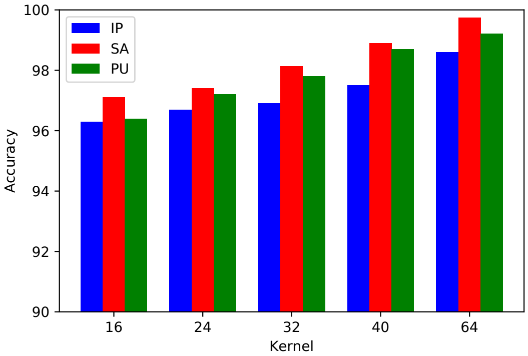

Fig. 3: The influence of OAs(%) with varying numbers of kernel for IP, UP and SA, respectively.

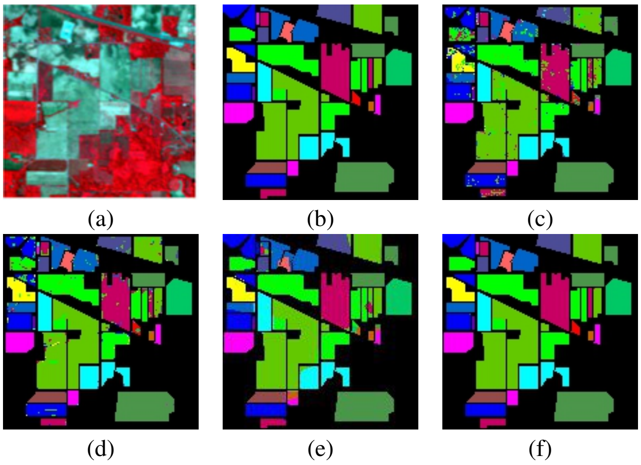

Fig. 4: The Classification Map for Indian Pines (a) False color image, (b) Ground Truth, (c)-(f) Predicted Classification Maps for 2D-CNN, 3D-CNN, SENet, and `FuSENet`, respectively.

both the spectral-spatial feature representation jointly. Which provides the discriminative information to accurately classify the target HSI data. The proposed `FuSENet` consistently outperform OAs as compared to the SENet(GAP) by average improvement of $+0.49$, $+1.12$, and $+0.12$ for IP, UP and SA respectively. The convergence of training losses shown in Fig. 9(a)-(c) and the convergence of the accuracies shown in Fig. 9(d)-(f) for IP, UP and SA using the proposed `FuSENet` framework and its different variations i.e., SENet (GAP) and SENet (GMP), respectively. It can be observed from the figures that the proposed model smoothly converge as compared to its other variants in both the scenario.

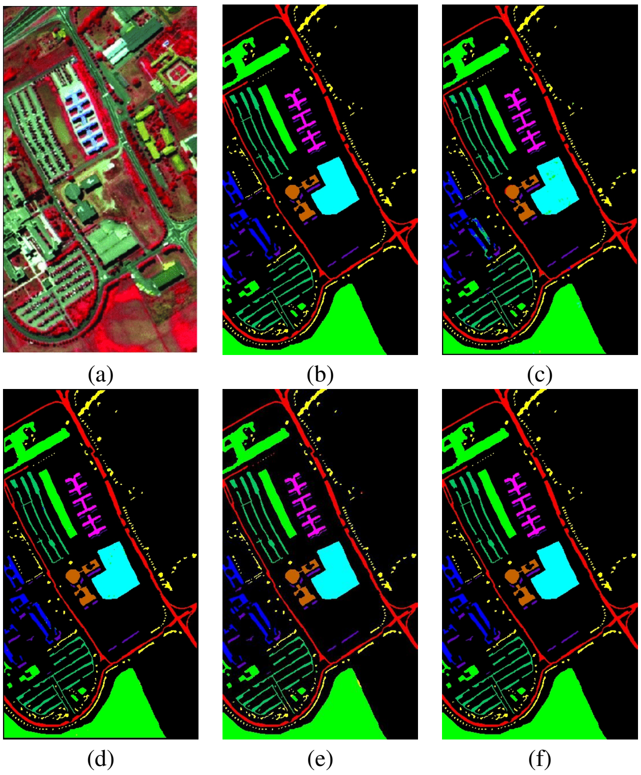

Fig. 5: The Classification Map for Pavia University (a) False color image, (b) Ground Truth, (c)-(f) Predicted Classification Maps for 2D-CNN, 3D-CNN, SENet, and `FuSENet`, respectively.

In order to explore the robustness of the proposed `FuSENet` Table 4 shows the classification performance of `FuSENet` in terms of OA, Kappa, and AA using varying training samples 10% and 20% over IP, UP and SA data sets, respectively.

The performance is reported in terms of the Overall Accuracy (OA), Average Accuracy (AA) and Kappa Coefficient. The best achieved results are highlighted in bold. It is observed from the experimental results that the proposed `FuSENet` outperforms other methods over each dataset in terms of each evaluation criteria. We also test the method simply using Global Average Pooling, i.e., SENet(GAP) and Global Max Pooling, i.e., SENet(GMP), respectively. Where we have found that the performance of fusion is significantly improved as compared to SENet methods due to the fact that fusion yields a better weight calibration feature maps at end. To validate the impact of different fusion techniques a comparison

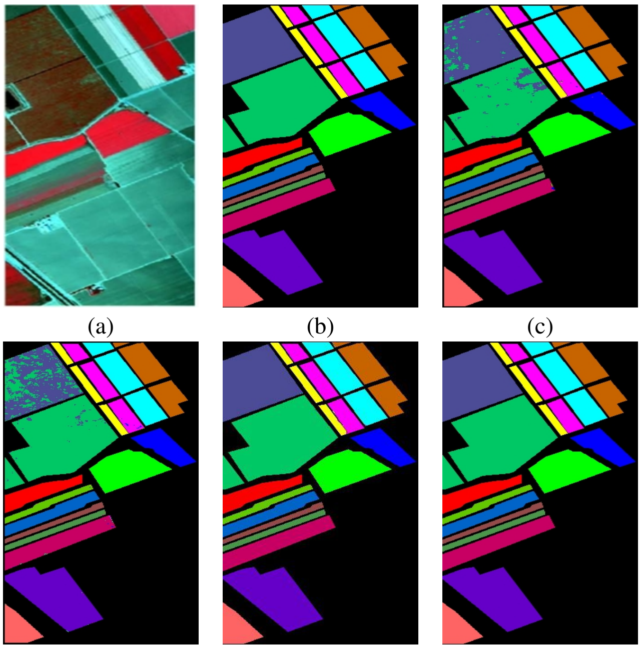
(a) (b) (c)

(d) (e) (f)

Fig. 6: The Classification Map for Salinas Scene (a) False color image, (b) Ground Truth, (c)-(f) Predicted Classification Maps for 2D-CNN, 3D-CNN, SENet, and `FuSENet`, respectively.

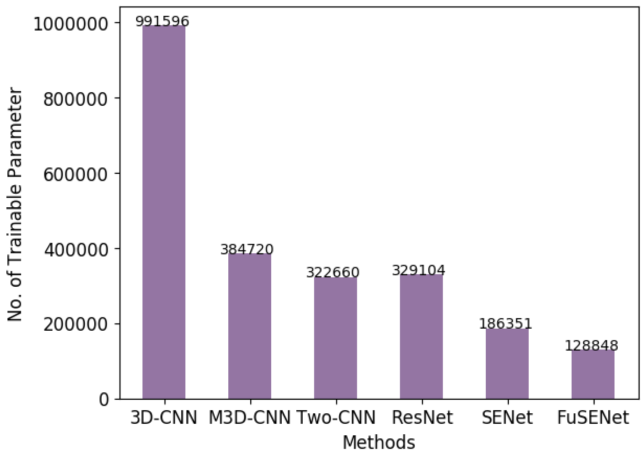

Fig. 8: The number of learnable model parameters for the the methods 3D-CNN, M3D-CNN, Two-CNN, ResNet, SENet, and `FuSENet`, respectively.

with other fusion strategies such as addition (Sum), multiplication ($Multiply$) and maximum (Max) are presented in Table 5. It is observed that the Max fusion is better suited for the proposed method and we prefer to use the maximum (Max) fusion strategy between the *sigmoid* output of GAP and GMP in proposed `FuSENet` method (shown in Fig. 1(c)).

The feature representation of any convolutional neural network (CNN) is always depends upon the convolutional filter banks and the ability to produce the discriminative feature maps be controlled by the number of kernel used in the filter banks. To show the impact of the number of kernels in the proposed network we varies the number of kernel from 16 to 64 and the step size is taken with power of 2 and shown in Fig. 3. It can be observed from Fig. 3 the model achieved highest classification performance with 64 kernels in each convolutional filter bank for IP, UP and SA, datasets respectively.

In order to well explore the impact of different spatial 3D input patches in the proposed `FuSENet` framework. Table 6 compares the performance of the proposed `FuSENet` framework in term of OAs, AAs, and kappa of the IN, UP, and SA datasets under different spatial input patches of size, 13 × 13 and 15 × 15, respectively. The results reported in Table 6, the proposed `FuSENet` framework shows sound classification performance for IP dataset when the spatial window of size was taken as 15 × 15 and it was 13 × 13 for UP and SA dataset in addition 20% of available labeled samples are supplied during training. The average OAs improved by the `FuSENet` are $+1.25$, $+0.35$, and 0.29 between the two spatial window of sizes 13 × 13 and 15 × 15 for IP, UP and SA datasets, respectively.

The visualization of the classification maps using different methods along with false color images, and their respective ground truth maps over the three datasets i.e., IP, UP and SA are shown in Fig. 4, 5, and 6 respectively. In addition the class legends of IP, UP and SA datasets are also shown in Fig. 7(a)-(c) . A quality classification map can be visualized using the proposed `FuSENet` method and which make sense from the quantitative comparison shown in Table 1, 2, and 3, respectively. The classification map generated through 3D-CNN is better as compared to SVM, and 2D-CNN but still their exist some artifacts within the class boundaries. This is mainly because of 2D-CNN uses only spatial information to predict the target pixels. During the training proposed `FuSENet` is capable to learn more discriminative and powerful spectral-spatial feature representations consecutively by simply “excite” the feature that helps in classification layer while suppress the ineffective feature based on the patterns produced by the `FuSENet` over the feature maps. So, the proposed `FuSENet` produces smooth and more accurate classification maps over all the HSI datasets as compared to the other methods.

To further analyse the classification performance shown in Table. 4 of the proposed FuSENet model we have conducted the one way statistical analysis of variance (ANOVA) test [45]. This ANOVA experiment is performed to explore the reason behind the improved classification performance achieved by FuSENet as compared to SVM, 3D-CNN, Two-CNN, DFeaFuNet, and SENet(GAP), respectively. The null hypothesis H_0 can determine *difference among group means is not significant* for the test. In an experiment if the p-value is lesser than the pre-selected significant level, which implies that at least one groups mean is significantly different from the others and we can simply reject the hypothesis H_0. The significance level is kept for the one way ANOVA test as α = 0.05 and the test results for three different datasets are shown in Table 7. In addition, the box plot corresponding to aforementioned ANOVA test for three

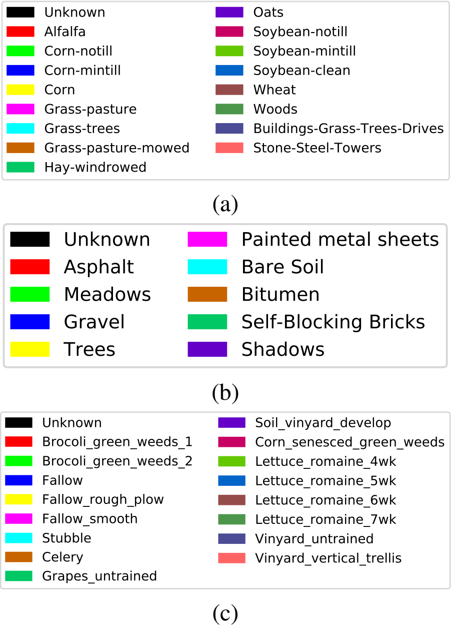

(a)

(b)

(c)

Fig. 7: The class legend for (a) Indian Pines (b) University of Pavia, and (c) Salinas Scene, datasets respectively, where black legend shows background class.

Table 7 One way statistical ANOVA test where the level of significance is selected as α = 0.05 for Indian Pines, University of Pavia, and Salinas Scene, respectively.

	Indian Pines Dataset				University of Pavia Dataset				Salinas Scene Dataset			
	Sum_Sq	**df**	**F**	**Prob(p)>F**	**Sum_Sq**	**df**	**F**	**Prob(p)>F**	**Sum_Sq**	**df**	**F**	**Prob(p)>F**
Groups	1570.418	5.0	5130.690	1.61e-35	212.725	5.0	514.927	1.37e-23	756.928	5.0	6490.738	9.60e-37
Residual	1.469	24.0			1.982	24.0			0.559	24.0		
Total	1571.88	29.0			214.708	29.0			757.48	29		

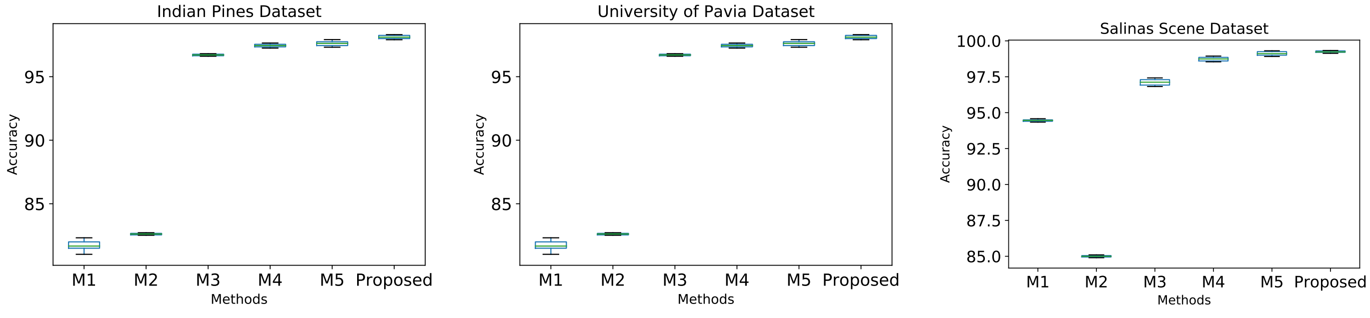

(a) (b) (c)

Fig. 9: (a)-(c) The box plot (methods vs. accuracy) of one way statistical ANOVA test for 'M1':SVM, 'M2':3D-CNN, 'M3':Two-CNN, 'M4':DFeaFuNet, 'M5':SENet(GAP) and proposed `FuSENet` models over IP, UP and SA datasets, respectively.

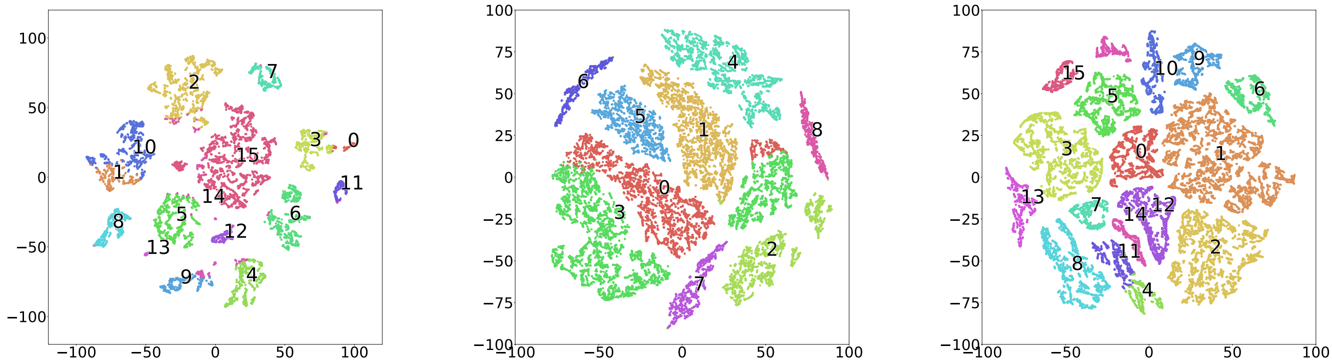

(a) (b) (c)

Fig. 10: Two-dimension spectral-spatial feature visualization of the proposed FuSENet via t-SNE where samples are represented through points and classes are shown in different colors for (a) Indian Pines, (b) University of Pavia, and (c) Salinas Scene datasets, respectively.

different datasets are also shown in Fig. 9(a)-(b), which clearly indicates that the mean performance of FuSENet is significantly better than the methods like SVM, 3D-CNN, Two-CNN, DFeaFuNet, and SENet(GAP), respectively.

To train a deep network it always require expensive hardware like GPUs and in the existing models million's of million's parameter need to be re-weights during training. Hence the number of parameter plays an important role while training. Fig. 8 shows the comparative distribution of learnable weigh parameters with the state-of-the-art methods i.e., 3D-CNN [41], M3D-CNN [42], Two-CNN [43], ResNet [38], SENet [4] and `FuSENet`, respectively. The proposed model contains less number of weight parameter as compared to others as observed from Fig. 8 and it is possible to train in a general configured machine with a minimum of 2GBs of graphical processing unit (GPUs). In order to increase feature generalization ability it is important to extract the joint spectral-spatial features simultaneously. Since the proposed `FuSENet` uses 3D residual learning block to extract joint spectral-spatial features and which ended with a high dimensional abstract representation of the feature and difficult to visualize within the high range. To visualize the discriminative power of the proposed feature representation, t-SNE [46] helps to transform the dimensionality of the learned features into 2D space and became much easier to plot. Fig. 10(a)-(c) show the t-SNE visualization of learned features in 2D for three HSI datasets i.e., IP, UP and SA, respectively. It can be clearly visualized from the figures that due to the use of large training epochs the learned spectral-spatial features from same class clustered together and features from different classes are became much easier to separate.

4 Conclusion

In this paper a CNN model named `FuSENet` is proposed in the SENet framework. To design the `FuSENet` we use two Squeeze and Excitation connection bi-linearly based on global average pooling (GAP) and global max pooling (GMP), respectively. To better utilizes both of the characteristic then fused the $sigmoid$ output of block SENet(GAP) and SENet(GMP) respectively, and compute the final scaling factor for each channel of input at any given layer. To enhance feature learning efficiency and avoid gradient vanishing problem the proposed `FuSENet` method is combined with 3D residual learning network and tested for Hyperspectral Image classification problem over three benchmark datasets. The results are compared with the state-of-the-art methods. The proposed `FuSENet` method has shown extremely good performance with a

© The Institution of Engineering and Technology 2019

limited amount of training data. It is also discovered that the Max fusion is better suited to the proposed `FuSENet` method.

5 References

1 Krizhevsky, A., Sutskever, I., Hinton, G.E. 'Imagenet classification with deep convolutional neural networks'. In: Advances in neural information processing systems. (, 2012. pp. 1097–1105

2 Russakovsky, O., Deng, J., Su, H., Krause, J., Satheesh, S., Ma, S., et al.: 'Imagenet large scale visual recognition challenge', *International journal of computer vision*, 2015, **115**, (3), pp. 211–252

3 He, K., Zhang, X., Ren, S., Sun, J. 'Deep residual learning for image recognition'. In: Proceedings of the IEEE conference on computer vision and pattern recognition. (, 2016. pp. 770–778

4 Hu, J., Shen, L., Sun, G. 'Squeeze-and-excitation networks'. In: Proceedings of the IEEE conference on computer vision and pattern recognition. (, 2018. pp. 7132–7141

5 Girshick, R., Donahue, J., Darrell, T., Malik, J. 'Rich feature hierarchies for accurate object detection and semantic segmentation'. In: Proceedings of the IEEE conference on computer vision and pattern recognition. (, 2014. pp. 580–587

6 Girshick, R. 'Fast r-cnn'. In: Proceedings of the IEEE international conference on computer vision. (, 2015. pp. 1440–1448

7 Ren, S., He, K., Girshick, R., Sun, J. 'Faster r-cnn: Towards real-time object detection with region proposal networks'. In: Advances in neural information processing systems. (, 2015. pp. 91–99

8 He, K., Gkioxari, G., Dollár, P., Girshick, R. 'Mask r-cnn'. In: Computer Vision (ICCV), 2017 IEEE International Conference on. (IEEE, 2017. pp. 2980–2988

9 Dubey, S.R., Roy, S.K., Chakraborty, S., Mukherjee, S., Chaudhuri, B.B.: 'Local bit-plane decoded convolutional neural network features for biomedical image retrieval', *Neural Computing and Applications*, , pp. 1–13

10 Repala, V.K., Dubey, S.R.: 'Dual cnn models for unsupervised monocular depth estimation', *arXiv preprint arXiv:180406324*, 2018,

11 Roy, S.K., Krishna, G., Dubey, S.R., Chaudhuri, B.B.: 'Hybridsn: Exploring 3-d-2-d cnn feature hierarchy for hyperspectral image classification', *IEEE Geoscience and Remote Sensing Letters*, 2019,

12 Akbari, D.: 'Improved neural network classification of hyperspectral imagery using weighted genetic algorithm and hierarchical segmentation', *IET Image Processing*, 2019, **13**, (12), pp. 2169–2175

13 Basha, S.S., Ghosh, S., Babu, K.K., Dubey, S.R., Pulabaigari, V., Mukherjee, S. 'Rccnet: An efficient convolutional neural network for histological routine colon cancer nuclei classification'. In: 2018 15th International Conference on Control, Automation, Robotics and Vision (ICARCV). (IEEE, 2018. pp. 1222–1227

14 Moradi, R., Berangi, R., Minaei, B.: 'Orthomaps: an efficient convolutional neural network with orthogonal feature maps for tiny image classification', *IET Image Processing*, 2019, **13**, (12), pp. 2067–2076

15 Jin, Y., Jiang, X.B., Wei, Z.k., Li, Y.: 'Chest x-ray image denoising method based on deep convolution neural network', *IET Image Processing*, 2019, **13**, (11), pp. 1970–1978

16 Liao, J., Li, B., Yang, D., Wang, J., Qi, Q., Wang, J.: 'Deep supervised hashing network with integrated regularisation', *IET Image Processing*, 2019,

17 Ahmad, M., Khan, A.M., Hussain, R.: 'Graph-based spatial–spectral feature learning for hyperspectral image classification', *IET image processing*, 2017, **11**, (12), pp. 1310–1316

18 Shamsolmoali, P., Zareapoor, M., Yang, J.: 'Convolutional neural network in network (cnnin): hyperspectral image classification and dimensionality reduction', *IET Image Processing*, 2018, **13**, (2), pp. 246–253

19 Khammari, M.: 'Robust face anti-spoofing using cnn with lbp and wld', *IET Image Processing*, 2019, **13**, (11), pp. 1880–1884

20 Nagpal, C., Dubey, S.R. 'A performance evaluation of convolutional neural networks for face anti spoofing'. In: 2019 International Joint Conference on Neural Networks (IJCNN). (IEEE, 2019. pp. 1–8

21 Roy, S.K., Dubey, S.R., Chanda, B., Chaudhuri, B.B., Ghosh, D.K. 'Texfusionnet: An ensemble of deep cnn feature for texture classification'. In: Proceedings of 3rd International Conference on Computer Vision and Image Processing. (Springer, 2020. pp. 271–283

22 Xie, S., Girshick, R., Dollár, P., Tu, Z., He, K. 'Aggregated residual transformations for deep neural networks'. In: Proceedings of the IEEE conference on computer vision and pattern recognition. (, 2017. pp. 1492–1500

23 Huang, G., Liu, Z., Van.Der.Maaten, L., Weinberger, K.Q. 'Densely connected convolutional networks'. In: Proceedings of the IEEE conference on computer vision and pattern recognition. (, 2017. pp. 4700–4708

24 Roy, S.K., Manna, S., Dubey, S.R., Chaudhuri, B.B.: 'Lisht: Non-parametric linearly scaled hyperbolic tangent activation function for neural networks', *arXiv preprint arXiv:190105894*, 2019,

25 Dubey, S.R., Chakraborty, S., Roy, S.K., Mukherjee, S., Singh, S.K., Chaudhuri, B.B.: 'diffgrad: An optimization method for convolutional neural networks', *arXiv preprint arXiv:190911015*, 2019,

26 Tu, B., Zhang, X., Kang, X., Zhang, G., Wang, J., Wu, J.: 'Hyperspectral image classification via fusing correlation coefficient and joint sparse representation', *IEEE Geoscience and Remote Sensing Letters*, 2018, **15**, (3), pp. 340–344

27 Ramesh, H.J..Z.G..T.M..B.: 'Vehicle detection in remote sensing images leveraging on simultaneous super-resolution', *IEEE Geoscience and Remote Sensing Letters*, 2019 (In press),

28 Chen, J., Wan, L., Zhu, J., Xu, G., Deng, M.: 'Multi-scale spatial and channel-wise attention for improving object detection in remote sensing imagery', *IEEE Geoscience and Remote Sensing Letters*, 2019 (In press),

29 Li, W., Chen, C., Zhang, M., Li, H., Du, Q.: 'Data augmentation for hyperspectral image classification with deep cnn', *IEEE Geoscience and Remote Sensing Letters*, 2018,

30 Fang, L., Liu, Z., Song, W.: 'Deep hashing neural networks for hyperspectral image feature extraction', *IEEE Geoscience and Remote Sensing Letters*, 2019, pp. 1–5

31 Li, S., Song, W., Fang, L., Chen, Y., Ghamisi, P., Benediktsson, J.A.: 'Deep learning for hyperspectral image classification: An overview', *IEEE Transactions on Geoscience and Remote Sensing*, 2019,

32 Kang, X., Zhuo, B., Duan, P.: 'Dual-path network-based hyperspectral image classification', *IEEE Geoscience and Remote Sensing Letters*, 2018,

33 Yu, Y., Gong, Z., Wang, C., Zhong, P.: 'An unsupervised convolutional feature fusion network for deep representation of remote sensing images', *IEEE Geoscience and Remote Sensing Letters*, 2018, **15**, (1), pp. 23–27

34 Song, W., Li, S., Fang, L., Lu, T.: 'Hyperspectral image classification with deep feature fusion network', *IEEE Transactions on Geoscience and Remote Sensing*, 2018, **56**, (6), pp. 3173–3184

35 Wang, L., Peng, J., Sun, W.: 'Spatial–spectral squeeze-and-excitation residual network for hyperspectral image classification', *Remote Sensing*, 2019, **11**, (7), pp. 884

36 Roy, S.K., Chatterjee, S., Bhattacharyya, S., Chaudhuri, B.B., Platoš, J.: 'Lightweight spectral-spatial squeeze-and-excitation residual bag-of-features learning for hyperspectral classification', *IEEE Transactions on Geoscience and Remote Sensing*, 2020,

37 Ioffe, S., Szegedy, C. 'Batch normalization: Accelerating deep network training by reducing internal covariate shift'. In: International Conference on Machine Learning. (, 2015. pp. 448–456

38 He, K., Zhang, X., Ren, S., Sun, J. 'Deep residual learning for image recognition'. In: Proceedings of the IEEE conference on computer vision and pattern recognition. (, 2016. pp. 770–778

39 Melgani, F., Bruzzone, L.: 'Classification of hyperspectral remote sensing images with support vector machines', *IEEE Transactions on geoscience and remote sensing*, 2004, **42**, (8), pp. 1778–1790

40 Makantasis, K., Karantzalos, K., Doulamis, A., Doulamis, N. 'Deep supervised learning for hyperspectral data classification through convolutional neural networks'. In: IEEE International Geoscience and Remote Sensing Symposium(IGARSS). (IEEE, 2015. pp. 4959–4962

41 Ben.Hamida, A., Benoit, A., Lambert, P., Ben.Amar, C.: '3-d deep learning approach for remote sensing image classification', *IEEE Transactions on geoscience and remote sensing*, 2018, **56**, (8), pp. 4420–4434

42 He, M., Li, B., Chen, H. 'Multi-scale 3d deep convolutional neural network for hyperspectral image classification'. In: IEEE International Conference on Image Processing (ICIP). (, 2017. pp. 3904–3908

43 Yang, J., Zhao, Y.Q., Chan, J.C.W.: 'Learning and transferring deep joint spectral–spatial features for hyperspectral classification', *IEEE Transactions on Geoscience and Remote Sensing*, 2017, **55**, (8), pp. 4729–4742

44 Green, R.O., Eastwood, M.L., Sarture, C.M., Chrien, T.G., Aronsson, M., Chippendale, B.J., et al.: 'Imaging spectroscopy and the airborne visible/infrared imaging spectrometer (aviris)', *Remote sensing of environment*, 1998, **65**, (3), pp. 227–248

45 Anscombe, F.: 'The validity of comparative experiments', *Journal of the royal statistical society series A (General)*, 1948, **111**, (3), pp. 181–211

46 Maaten, L.v.d., Hinton, G.: 'Visualizing data using t-sne', *Journal of machine learning research*, 2008, **9**, (Nov), pp. 2579–2605

© The Institution of Engineering and Technology 2019